



# Fungal effector SIB1 of *Colletotrichum orbiculare* has unique structural features and can suppress plant immunity in *Nicotiana benthamiana*

Received for publication, July 1, 2021, and in revised form, October 21, 2021 · Published, Papers in Press, October 29, 2021,  
<https://doi.org/10.1016/j.jbc.2021.101370>

Ru Zhang<sup>1,‡</sup>, Noriyoshi Isozumi<sup>2,‡</sup>, Masashi Mori<sup>3,\*</sup>, Ryuta Okuta<sup>1</sup>, Suthitar Singkaravanit-Ogawa<sup>1</sup>,  
Tomohiro Imamura<sup>3</sup>, Jun-Ichi Kurita<sup>4</sup>, Pamela Gan<sup>5</sup>, Ken Shirasu<sup>5</sup> , Shinya Ohki<sup>2,\*</sup> , and Yoshitaka Takano<sup>1,\*</sup> 

From the <sup>1</sup>Graduate School of Agriculture, Kyoto University, Kyoto, Japan; <sup>2</sup>Center for Nano Materials and Technology (CNMT), Japan Advanced Institute of Science and Technology (JAIST), Ishikawa, Japan; <sup>3</sup>Research Institute for Bioresources and Biotechnology, Ishikawa Prefectural University, Ishikawa, Japan; <sup>4</sup>Graduate School of Medical Life Science, Yokohama City University, Yokohama, Japan; <sup>5</sup>Center for Sustainable Resource Science, RIKEN, Yokohama, Japan

Edited by Joseph Jez

Fungal plant pathogens secrete virulence-related proteins, called effectors, to establish host infection; however, the details are not fully understood yet. Functional screening of effector candidates using *Agrobacterium*-mediated transient expression assay in *Nicotiana benthamiana* identified two virulence-related effectors, named SIB1 and SIB2 (Suppression of Immunity in *N. benthamiana*), of an anthracnose fungus *Colletotrichum orbiculare*, which infects both cucurbits and *N. benthamiana*. The *Agrobacterium*-mediated transient expression of SIB1 or SIB2 increased the susceptibility of *N. benthamiana* to *C. orbiculare*, which suggested these effectors can suppress immune responses in *N. benthamiana*. The presence of SIB1 and SIB2 homologs was found to be limited to the genus *Colletotrichum*. SIB1 suppressed both (i) the generation of reactive oxygen species triggered by two different pathogen-associated molecular patterns, chitin and flg22, and (ii) the cell death response triggered by the *Phytophthora infestans* INF1 elicitor in *N. benthamiana*. We determined the NMR-based structure of SIB1 to obtain its structural insights. The three-dimensional structure of SIB1 comprises five  $\beta$ -strands, each containing three disulfide bonds. The overall conformation was found to be a cylindrical shape, such as the well-known antiparallel  $\beta$ -barrel structure. However, the  $\beta$ -strands were found to display a unique topology, one pair of these  $\beta$ -strands formed a parallel  $\beta$ -sheet. These results suggest that the effector SIB1 present in *Colletotrichum* fungi has unique structural features and can suppress pathogen-associated molecular pattern-triggered immunity in *N. benthamiana*.

(PAMPs), which are often present on their external face. Plant recognition of PAMPs triggers pathogen-associated molecular pattern-triggered immunity (PTI). Although the plant immune system against most potential pathogenic microbes, especially nonadapted pathogens, is thought to depend mainly on PTI, adapted pathogens have evolved various mechanisms to suppress PTI (3). The secreted virulence factors, called effectors, play important roles in the suppression of PTI. In response to a pathogen's use of effectors to try to suppress PTI, plants actuate their second layer of defense, called effector-triggered immunity (4). Effector-triggered immunity induces strong and robust immune responses that are typically associated with programmed cell death (PCD), a response referred to as the hypersensitive response (HR).

Members of the ascomycete genus *Colletotrichum* include numerous species that can infect a wide range of plant species, including many commercially important cultivars (5–7). The lifestyle of *Colletotrichum* species is considered to be hemibiotrophic, which combines an initial short biotrophic phase to maintain live host tissue and a subsequent necrotrophic phase that kills host tissue. In general, *Colletotrichum* fungi develop a specialized infection structure called appressorium that is darkly pigmented with melanin, and melanized appressorium is important for host penetration (8, 9). Genome analyses have identified numerous effector candidate genes in *Colletotrichum* fungi such as *Colletotrichum higginsianum* and *Colletotrichum orbiculare* (5, 6).

*C. orbiculare* belongs to the orbiculare clade (or called the *C. orbiculare* species complex) and infects multiple cucurbitaceous cultivars (9–11). Interestingly, *C. orbiculare* can also infect *Nicotiana benthamiana*, which belongs to the Solanaceae family but is distant from cucurbits (12–14). We previously reported on the virulence-related effectors NIS1 and CoDN3 of *C. orbiculare* that are preferentially expressed in the biotrophic phase (15, 16). We revealed that the expression of NIS1 leads to PCD in *N. benthamiana*, and that the NIS1-triggered PCD is suppressed by CoDN3 expression (16). CoDN3 also inhibits PCD in *N. benthamiana* induced by another *C. orbiculare* effector NLP1 (17). We recently reported

Plants use multilayered strategies to detect and defeat pathogenic microbes trying to attack them (1, 2). As the first layer of plant defense, plants recognize conserved components of microbes called pathogen-associated molecular patterns

<sup>‡</sup> These authors contributed equally to this work.

\* For correspondence: Yoshitaka Takano, [takano.yoshitaka.2x@kyoto-u.ac.jp](mailto:takano.yoshitaka.2x@kyoto-u.ac.jp); Shinya Ohki, [shinya-o@jaist.ac.jp](mailto:shinya-o@jaist.ac.jp); Masashi Mori, [mori@ishikawa-pu.ac.jp](mailto:mori@ishikawa-pu.ac.jp).

## Effector with unique structure suppresses plant immunity

that NIS1 targets *Arabidopsis thaliana* BAK1 and BIK1, which function in PAMP recognition and subsequent PTI activation, together with pattern recognition receptors that sense particular PAMPs (18).

We have previously reported that both adapted and non-adapted *Colletotrichum* fungi commonly develop melanized appressoria on *Arabidopsis* at 1 day post inoculation (1 dpi) (19). However, melanized appressoria of the adapted *Colletotrichum* fungus develop invasive hyphae successfully, whereas those of nonadapted *Colletotrichum* fungi fail to develop invasive hyphae because *Arabidopsis* plants activate a pre-invasive defense (19). The finding therefore suggested that melanized appressoria of *Colletotrichum* fungi likely secrete effectors that are critical for the suppression of preinvasive plant defense. Consistently, microarray-based expression analysis of *C. orbiculare* inoculated on *N. benthamiana* shows that many small and secreted protein genes are highly expressed at 1 dpi, when the pathogen has developed melanized appressoria but has not yet formed invasive hyphae (5).

In this study, to identify novel virulence-related effectors of *C. orbiculare*, we focused on the effector-like genes expressed at 1 dpi after inoculation of *C. orbiculare* on *N. benthamiana*. Using the newly obtained RNA sequence data derived from *N. benthamiana* inoculated with *C. orbiculare* at 1 dpi, we selected candidate effector-like genes of *C. orbiculare* and subjected them to a functional screening assay via *Agrobacterium*-mediated transient expression. Each candidate was transiently expressed in *N. benthamiana* leaves that were subsequently challenged with *C. orbiculare* to assess each candidate's ability to suppress the immunity of *N. benthamiana*. In these experiments, we identified two novel virulence-related effectors, named SIB1 and SIB2 (Suppression of Immunity in *N. benthamiana*), that suppressed *N. benthamiana* immunity against *C. orbiculare*. We then performed further characterization of SIB1. Transient expression of SIB1 suppressed both (i) the generation of reactive oxygen species (ROS) triggered by two different PAMPs, chitin and flg22, and (ii) the cell death response triggered by the *Phytophthora infestans* INF1 elicitor. We next determined the tertiary structure of SIB1 to obtain structural insights into this effector. Using NMR analysis, we have solved the tertiary structure of SIB1, which showed that the effector SIB1 of *C. orbiculare* has unique structural features.

## Results

### Functional screening of virulence-related effectors in *C. orbiculare*

We obtained RNA sequence data from the following: (i) *N. benthamiana* leaves inoculated with *C. orbiculare* at 1, 3, and 7 dpi; (ii) conidia of *C. orbiculare*, and (iii) *in vitro* grown hyphae of *C. orbiculare*. We ranked the putative secreted protein genes of *C. orbiculare* based on their expression in *N. benthamiana* at 1 dpi (Table S1). The list included NIS1 and CAD1, which we have previously studied (18, 20). We then selected eight candidates, named CE1 to CE8 (Table S1), from the list, and these selected candidates were subjected to further

functional screening. As mentioned previously, *C. orbiculare* infects and causes lesions in *N. benthamiana* (13, 14). In a study using a functional assay based on the *Agrobacterium*-mediated transient expression of NIS1 in *N. benthamiana* and subsequent inoculation with *C. orbiculare*, we recently reported that the expression of the effector NIS1 in *N. benthamiana* increased its susceptibility to *C. orbiculare* (18). We applied this assay to the functional screening of the selected candidates.

We expressed each candidate in *N. benthamiana* by transient expression using *Agrobacterium* infiltration, and we challenged the expression sites of each candidate by inoculation with *C. orbiculare*. The expression of CE6 caused lesion development before *C. orbiculare* inoculation, suggesting that CE6 can induce cell death in *N. benthamiana* (Fig. S1). The other candidates did not cause lesion development before *C. orbiculare* inoculation. Notably, we found that the expression of two candidates (CE7 and CE5) in *N. benthamiana* increased its susceptibility to *C. orbiculare* (Fig. 1, A and B). Expression of the other candidates had no obvious effect on the susceptibility to *C. orbiculare*. These results suggest that CE7 and CE5 can suppress plant immunity of *N. benthamiana* against *C. orbiculare*.

We named CE7 and CE5 as SIB1 and SIB2, respectively. SIB1 (GenBank accession number: TDZ19150.1) encodes a protein of 70 amino acids that had no significant matches in a Pfam search. SignalP analysis has suggested that SIB1 has a signal peptide of 20 amino acids (21) (Fig. 1C). SIB2 (GenBank accession number: TDZ19243.1) encodes a protein of 99 amino acids that includes a signal peptide of 18 amino acids but has no clear domains as shown in a Pfam search. We then performed BlastP against the National Center for Biotechnology Information nonredundant protein database using SIB1 and SIB2 as the query sequences (Fig. S2). We found homologs of SIB1 (100% identity in amino acid sequence) in *Colletotrichum spinosum*, *Colletotrichum trifolii*, and *Colletotrichum sidae* that are members of the orbiculare clade that *C. orbiculare* belongs to. In contrast, genes predicted to encode full-length SIB2 homologs were only identified in *C. spinosum* and *C. trifolii* but not in *C. sidae*. Homologs of both SIB1 and SIB2 were also found in a subset of *Colletotrichum* species outside the orbiculare clade but were not found outside the *Colletotrichum* genus (Fig. S2).

### Suppression by SIB1 of multiple PTI responses in *N. benthamiana*

We decided to focus on SIB1 and performed further characterization of this novel effector. We will report further studies on CE6 and SIB2 elsewhere. To investigate whether SIB1 suppresses PAMP-triggered ROS generation in *N. benthamiana*, we measured the ROS generation triggered by two PAMPs, chitin (a fungal PAMP) and flg22 (a bacterial PAMP), in *N. benthamiana* expressing SIB1. It was recently reported that the NIS1 of *C. orbiculare* and an NIS1 homolog of *Magnaporthe oryzae* (MoNIS1) commonly suppress ROS production triggered by both chitin and flg22 in

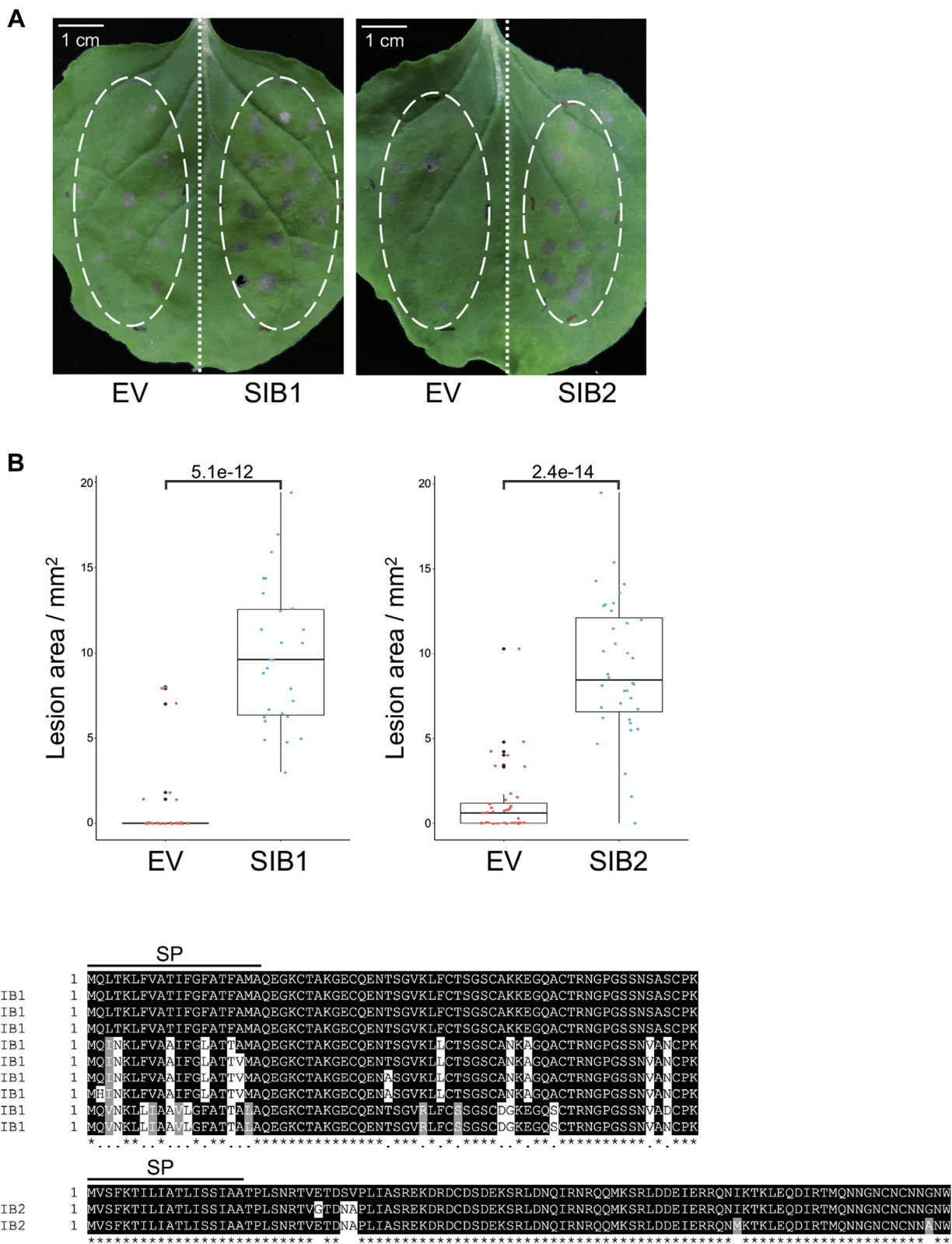


**Figure 1. Transient expression of the effector SIB1 or SIB2 in *Nicotiana benthamiana* decreased immunity to *Colletotrichum orbiculare*.** A, increased lesion development of *C. orbiculare* on *N. benthamiana* when SIB1 or SIB2 were transiently expressed. *N. benthamiana* leaves were infiltrated by *Agrobacterium tumefaciens* harboring the plasmid expressing SIB1, the plasmid expressing SIB2, or the empty plasmid (EV), and the infiltrated leaves were incubated for 2 days and then drop-inoculated with conidial suspensions ( $5 \times 10^5$  conidia/ml) of *C. orbiculare* 104-T. The photograph was taken at 5 dpi. Similar results were obtained from two additional experiments. B, quantification of lesion size on *N. benthamiana* leaves transiently expressing SIB1 or SIB2 after *C. orbiculare* inoculation. The lesion size in A was measured using ImageJ software for three biological replicates. Centerlines show the medians. Black dots represent outliers. Individual data points are plotted as colored dots. The *t* test was used to identify significant differences. C, SIB1 and SIB2 are conserved in *Colletotrichum* species. The amino acid sequence alignments of SIB1 or SIB2 with their orthologs of *Colletotrichum* species were shown. The

## Effector with unique structure suppresses plant immunity

*N. benthamiana* (18); therefore, we also investigated the ROS production triggered by these PAMPs in the presence of MoNIS1. Both SIB1 and MoNIS1 suppressed the ROS production triggered by chitin and flg22, in contrast with the negative control enhanced GFP (eGFP) (Fig. 2, A and B), which suggests that SIB1 can suppress one of the typical PTI responses.

Some effectors have been shown to increase the virulence of a pathogen by suppressing the HR, which is accompanied by cell death (22). *P. infestans* INF1 is a well-known oomycete PAMP elicitor that can induce the HR in *N. benthamiana* leaves (23). NIS1 and MoNIS1 also suppress INF1-induced HR cell death in *N. benthamiana* (18). To investigate whether SIB1 can interfere with cell death triggered by the PAMP elicitor, SIB1, MoNIS1, or eGFP was expressed in *N. benthamiana* using *Agrobacterium* infiltration, and the infiltration sites were challenged with *Agrobacterium* carrying *INF1*. INF1-triggered lesion development was observed in the infiltration sites expressing GFP but was clearly suppressed in the sites expressing MoNIS1 as previously shown. Notably, SIB1 also suppressed INF1-induced lesion development, which indicated that SIB1 suppresses HR cell death triggered by the PAMP elicitor INF1 (Fig. 2C). These findings suggest that the effector SIB1 can suppress multiple PTI responses in *N. benthamiana*.

We next performed RT-quantitative PCR (qPCR) analysis to investigate the expression pattern of *SIB1* in conidia of *C. orbiculare* inoculated on *N. benthamiana* and cucumber. The expression of *SIB1* at 0, 24, and 72 h post inoculation (hpi) of *C. orbiculare* on *N. benthamiana* was consistent with the RNA sequence data (conidia, 1 dpi in *N. benthamiana*, and 3 dpi in *N. benthamiana*) (Table S1). *SIB1* expression started to be induced at 8 hpi, and its expression level was highest at 12 hpi (Fig. 3A). *SIB1* expression was induced after inoculation on cucumber (Fig. 3A). However, the expression pattern of *SIB1* on cucumber was not identical to that on *N. benthamiana* (Fig. 3A); for example, *SIB1* expression was highly induced at 72 hpi on cucumber but not on *N. benthamiana*.

We next applied targeted gene disruption of *SIB1* and investigated whether *SIB1* is required for the virulence of *C. orbiculare*. To delete *SIB1* in *C. orbiculare*, we first generated the *lig4* $\Delta$  strain from *C. orbiculare* 104-T, in which an increased homologous recombination ratio is expected (24), and used the *lig4* $\Delta$  strain as the parental strain for the gene disruption of *SIB1* (details are included in the Experimental procedures section). The *SIB1*-knockout vector, named pCB1636SIB1, was constructed and introduced into the *lig4* $\Delta$  strain, and knockout mutants of *SIB1* were obtained (Figs. S3A and 3B). The colony morphology and conidiogenesis of the generated *SIB1*-knockout mutants (*sib1* $\Delta$ ) on potato dextrose agar (PDA) medium were similar to those of the control

parental strain (Fig. S3C). We then inoculated the *sib1* $\Delta$  strains on *N. benthamiana*, cucumber, and melon and found that the *sib1* $\Delta$  strains developed the same lesions as the control strain for all plants tested (Fig. 3B).

### Post-transcriptional modification of SIB1

We next focused on the structural aspects of the effector SIB1. We tried to produce SIB1 protein in the suspension-cultured *Nicotiana tabacum* cv. Bright Yellow 2 (BY-2) system (25, 26), in which the research target protein is expressed as a fused protein together with both tobamovirus (ToMV) and transcription factor (XVE) to increase the productivity. This system also uses optimized signal peptides for endoplasmic reticulum migration and secretion to fold the yielded protein. The system can produce proteins containing disulfide bonds in their native conformation (27–30). We used this system to prepare SIB1, whose amino acid sequence has six Cys residues that are expected to form intramolecular disulfide bonds.

We prepared semipurified SIB1 protein. When all Cys residues are in reduced form, the theoretical mass of SIB1 is calculated as 5396.388 *m/z*. We treated the purified SIB1 as for the reduced form and confirmed the mass. As shown in Figure 4A (upper panel), the mass of the reduced SIB1 (5378.586 *m/z*) was slightly smaller than the theoretical value of 5396.388 *m/z*, which suggests that the SIB1 expressed by the BY-2 system had some modification. A search of the Unimod database suggested that the difference (–17.802 *m/z*) is derived from pyroglutamylation of the N-terminal residue, Gln1. To confirm the pyroglutamylation of SIB1, we used pyroglutamate aminopeptidase (PGAP) treatment of SIB1. Because only N-terminal pyroglutamic acid is cleaved by this treatment, we used this assay to determine whether the sample protein contained N-terminal pyroglutamic acid. For the PGAP-treated sample (Fig. 4A, lower panel), only the peak (5267.895 *m/z*), which corresponds to the N-terminal glutamine-cleaved SIB1 ( $\Delta$ Q1-SIB1), was detected. The MS results showed clearly that the N-terminal residue of SIB1 expressed in BY-2 cells was pyroglutamic acid. The Gln at the N-terminal end was easily modified to pyroglutamic acid (31, 32).

The mass of pyroglutamylated SIB1 suggested that all Cys residues were in the oxidized form, as shown in Figure 4B. Therefore, we used MS to analyze the disulfide bond pairs. Lys-C treatment under nonreducing conditions caused SIB1 digestion, but the disulfide bonds were maintained. As shown in Figure 4B, we observed four peaks for the Lys-C-treated sample: one peak (5031.432 *m/z*) corresponding to undigested SIB1 and three other peaks (1014.473 *m/z*, 1949.780 *m/z*, and 2077.858 *m/z*) indicating digested peptides containing disulfide linkages. Further MS analysis of the products of the

alignments include the orthologs showing more than 75% amino acid identity obtained using a BlastP search of the National Center for Biotechnology Information nonredundant protein database using SIB1 or SIB2 as the query sequences. They were derived from the diverse *Colletotrichum* species represented by *Cspi* (*C. spinosum*), *Ctri* (*C. trifolii*), *Csid* (*C. sidae*), *Ccam* (*C. camelliae*), *Casi* (*C. asianum*), *Cfru* (*C. fruticola*), *Caen* (*C. aenigma*), *Csco* (*C. scovillei*), and *Cnym* (*C. nymphaeae*). The alignments were made using the ClustalW program. Identical residues in SIB1 or SIB2 are shaded in black, and conserved residues are shaded in gray. SP indicates the putative signal peptide region. SIB, Suppression of Immunity in *N. benthamiana*.

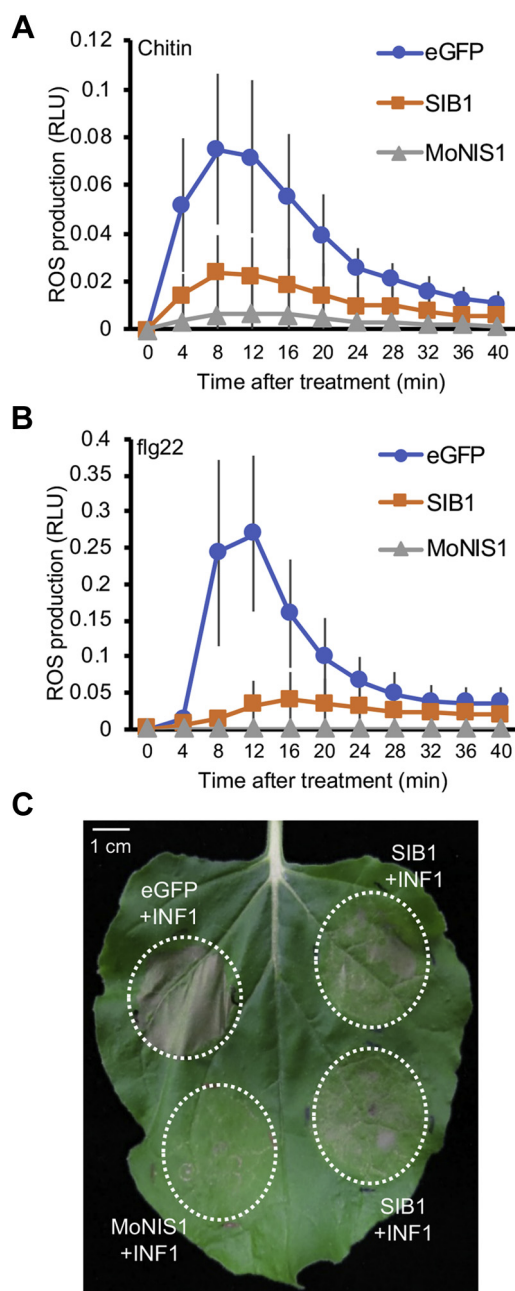


**Figure 2. SIB1 suppressed PAMP-triggered ROS generation and HR cell death in *Nicotiana benthamiana*.** *A*, chitin-triggered ROS production in *N. benthamiana* was inhibited by transient expression of *SIB1*. After treatment with 200  $\mu\text{g/ml}$  chitin, the total ROS production was measured in *N. benthamiana* transiently expressing *SIB1-HA*, or *MoNIS1-HA* (positive control), or *eGFP-HA* (negative control). Data are presented as mean  $\pm$  SE ( $n = 12$ ). Similar results were obtained from two additional experiments. *B*, flg22-triggered ROS production in *N. benthamiana* was inhibited by transient expression of *SIB1*. After treatment with 1  $\mu\text{M}$  flg22, the total ROS production was measured in *N. benthamiana* transiently expressing *SIB1-HA*, or *MoNIS1-HA* (positive control), or *eGFP-HA* (negative control). Data are presented as mean  $\pm$  SE ( $n = 12$ ). Similar results were obtained from two additional experiments. *C*, partial suppression of *INF1* induced cell death by *SIB1*. *N. benthamiana* leaves were first infiltrated with *Agrobacterium tumefaciens* harboring a plasmid expressing *SIB1*, *eGFP* (negative control), or *MoNIS1* (positive control). After 1 day, the second infiltration with *A. tumefaciens* harboring a plasmid expressing *INF1* was performed, and the infiltrated leaves were incubated for 5 days. Similar results were obtained from two additional experiments. HR, hypersensitive response; PAMP, pathogen-associated molecular pattern; ROS, reactive oxygen species; SIB, Suppression of Immunity in *N. benthamiana*.

enzymatic digestion clearly indicated the existence of two disulfide bonds, Cys22–Cys27 and Cys35–Cys48, as shown in Figure 4C. Peptides containing Cys5 and Cys11 were not detected, probably because of difficulty with their ionization. Because all Cys residues were in the oxidized form, as shown in Figure 4B, the remaining two Cys residues, Cys5 and Cys11, were expected to form disulfide bonds.

### Structure of SIB1

Unlabeled and  $^{15}\text{N}$ -labeled SIB1 samples were expressed in the BY-2 system, and the N terminus of NMR sample used in this study was pyroglutamylated. As shown in Fig. S4, the  $^1\text{H}$ - $^{15}\text{N}$  heteronuclear single quantum coherence spectrum of SIB1 showed well-dispersed signals with sharp line shapes, which indicated that SIB1 was in a stable conformation in solution. After the resonance assignments, three-dimensional structure calculation was performed with the distance and angle constraints derived from NMR data. Disulfide bond constraints for three Cys–Cys pairs were also used in the calculation. Preliminary three-dimensional structures were obtained with CYANA 2.1 (33) and PONDEROSA-C/S (34), and the refined structures in explicit water were calculated by using ARIA 2.2 (35) and XPLOR-NIH 3.3 (36). We finally obtained ten structures of SIB1 with  $0.59 \pm 0.09$  Å of root mean square deviation for backbone atoms of residues 2 to 49. The final structures showed no violation in distance ( $>0.5$  Å) or angle ( $>5^\circ$ ) restraints. The structural statistics are summarized in Table 1.

A backbone wire model of the final ensemble and a ribbon model of the representative model are shown in Figure 5, A and C, respectively. The three-dimensional structure of SIB1 comprised five  $\beta$ -strands without an  $\alpha$ -helix. The strands form a cylindrical shape, the so-called  $\beta$ -barrel. The five strands were named  $\beta 1$  to  $\beta 5$  starting from the N terminus span residue 2 to 6, 10 to 14, 18 to 23, 36 to 38, and 44 to 47, respectively. We found that the three-dimensional structure of SIB1 includes three disulfide bonds, all of which are located in the inner part of the molecule, as shown in Figure 5C.

The topology of the five  $\beta$ -strands is shown in Figure 5B. Although three pairs of the  $\beta$ -strands ( $\beta 1$ – $\beta 2$ ,  $\beta 2$ – $\beta 3$ , and  $\beta 4$ – $\beta 5$ ) are in the antiparallel orientation, only one pair,  $\beta 3$  to  $\beta 5$ , adopts a parallel form. This is a unique characteristic of SIB1 because the antiparallel  $\beta$ -barrel is the most common structure. A search using the structure comparison server DALI (<http://ekhidna2.biocenter.helsinki.fi/dali/>) suggested that no protein in the database displays the SIB1-like fold, five-strand  $\beta$ -barrel structure containing one parallel  $\beta$ -sheet. The highest Z-score of the DALI search was 3.6 found for a part of ribonuclease R (Protein Data Bank [PDB] code: 7DIC). As judged by the lower Z-score, the corresponding part requires several large gaps in the sequence and structural alignment with SIB1, suggesting their dissimilarity.

The electrostatic potential of the molecular surface of SIB1 is shown in Figure 5D. As seen in Figure 5D, molecular surface of SIB1 has a positively charged area composed of relatively

## Effector with unique structure suppresses plant immunity

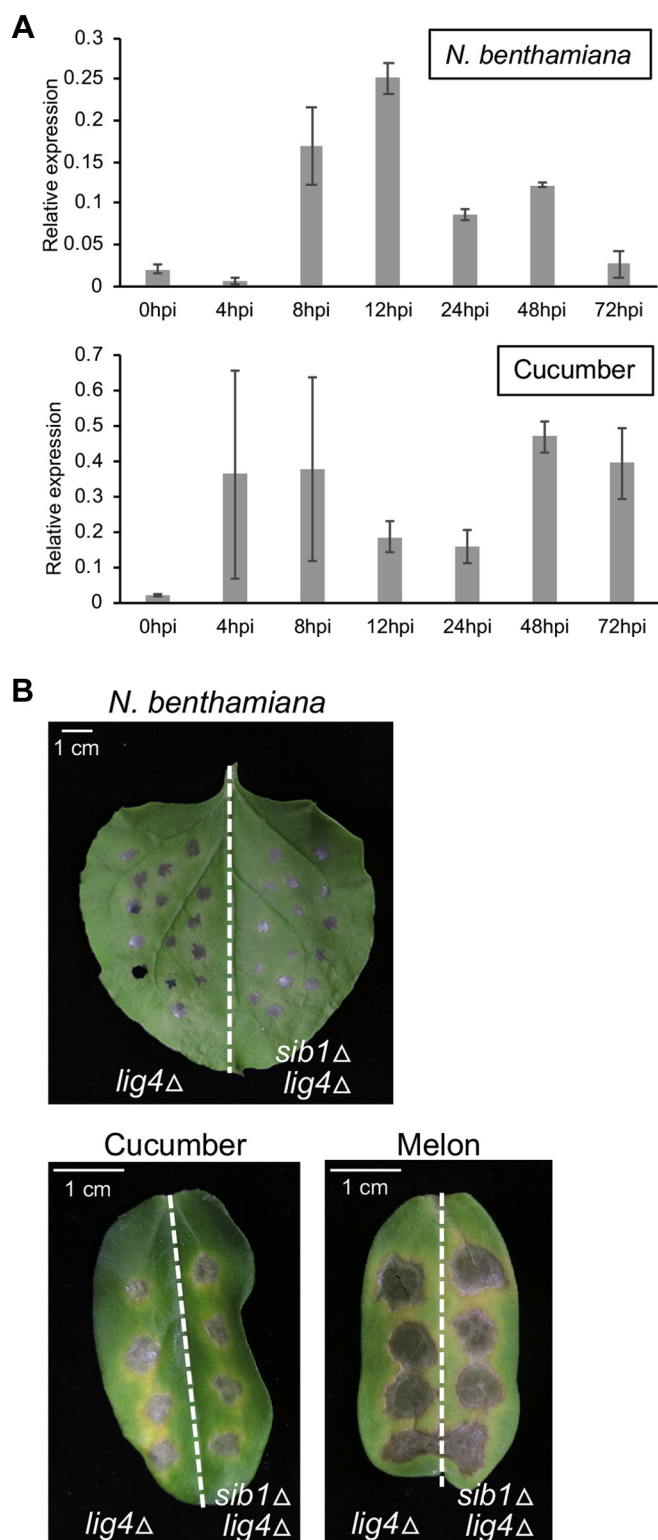


**Figure 3. Gene expression analysis of SIB1 and pathogenicity test of the SIB1 knockout mutants.** A, expression pattern of SIB1 in *Colletotrichum orbiculare* inoculated on *Nicotiana benthamiana* and cucumber. The conidial suspension of *C. orbiculare* wildtype strain ( $1 \times 10^6$  conidia per milliliter) was inoculated on *N. benthamiana* leaves or cucumber cotyledons. The total RNA of inoculated plants was extracted and subjected to RT-quantitative PCR analysis to investigate SIB1 expression. The *C. orbiculare* actin gene was used as the internal control. Mean and SD were calculated from three independent samples. Similar results were obtained from one additional experiment. B, gene disruption of SIB1 had no visible effects on the virulence of *C. orbiculare* inoculated on *N. benthamiana*, cucumber, or melon.

long side chains of K8, K19, K29, and K30. An intriguing surface property is seen at the top side of the  $\beta$ -barrel structure. A shallow bowl-like shape is formed by the loop between  $\beta 3$  and  $\beta 4$ . The central bed region of this area is positively charged K30, and this charge is surrounded by a hydrophobic rim.

As an additional analysis, we performed  $T_1$ ,  $T_2$ , and  $\{^1\text{H}\}-^{15}\text{N}$  NOESY experiments to obtain information about the dynamics of each residue. These results are shown in Fig. S5. All  $1/T_1$ ,  $1/T_2$ , and  $\{^1\text{H}\}-^{15}\text{N}$  NOE values indicated that the overall structure was rigid and stable in the NMR time scale. Slightly smaller  $\{^1\text{H}\}-^{15}\text{N}$  NOE values were observed only for the loop regions, which suggested that the loops are more flexible than the  $\beta$ -strand regions. Unlike the loop regions, relatively higher  $1/T_2$  values were observed for few residues located in the  $\beta$ -strands, but such residues appeared sporadically through the amino acid sequence. Moreover, the  $1/T_1$  and heteronuclear NOE did not show higher/lower values for such residues, indicating no further information about the rigidity. The analyses of the dynamics suggested that the poor plasticity of the SIB1 conformation makes it difficult to deduce the functional site involved in the conformational selection needed to adapt to the target. The classical key-and-lock binding manner might be proposed, but identification of the target binding region is not possible at present.

## Discussion

In this study, we selected effector candidate genes of *C. orbiculare* that were highly expressed at 1 dpi after inoculation of the pathogen on *N. benthamiana* and performed functional screening using an *Agrobacterium*-mediated transient expression assay in *N. benthamiana*. We identified CE6 as a factor that caused cell death in *N. benthamiana*. Importantly, we also identified two novel effectors of *C. orbiculare*, named SIB1 and SIB2, that suppressed *N. benthamiana* immunity against *C. orbiculare*. SIB1 was found to be conserved in the genome of 18 *Colletotrichum* species but was not found outside the *Colletotrichum* genus. Homologs encoding the amino acid sequence identical to that of *C. orbiculare* SIB1 were found in *C. spinosum*, *C. trifolii*, and *C. sidae*, which also belong to the orbiculare clade (37). SIB2 homologs were identified in the genome of 24 *Colletotrichum* species, including *C. spinosum* and *C. trifolii* but not in *C. sidae*.

We focused on SIB1 in this study. SIB1 suppressed the ROS burst triggered by both chitin and flg22 in *N. benthamiana*. Plant NADPH oxidases, also known as respiratory burst oxidase homologs (RBOHs), produce ROS (38). An RBOHB (NrRBOHB) of *N. benthamiana* plays crucial roles in ROS production triggered by PAMPs, such as bacterial flagellin and fungal chitin, and facilitates plant immunity against biotrophic

Conidial suspension ( $5 \times 10^5$  conidia/ml) of the parental *lig4* $\Delta$  strain or the *sib1* $\Delta$  strain (*lig4* $\Delta$  background) was drop-inoculated on *N. benthamiana* leaves, cucumber cotyledons, and melon cotyledons, and the inoculated plants were incubated at 24 °C for 7 days. Similar results were obtained from two additional experiments. SIB, Suppression of Immunity in *N. benthamiana*.

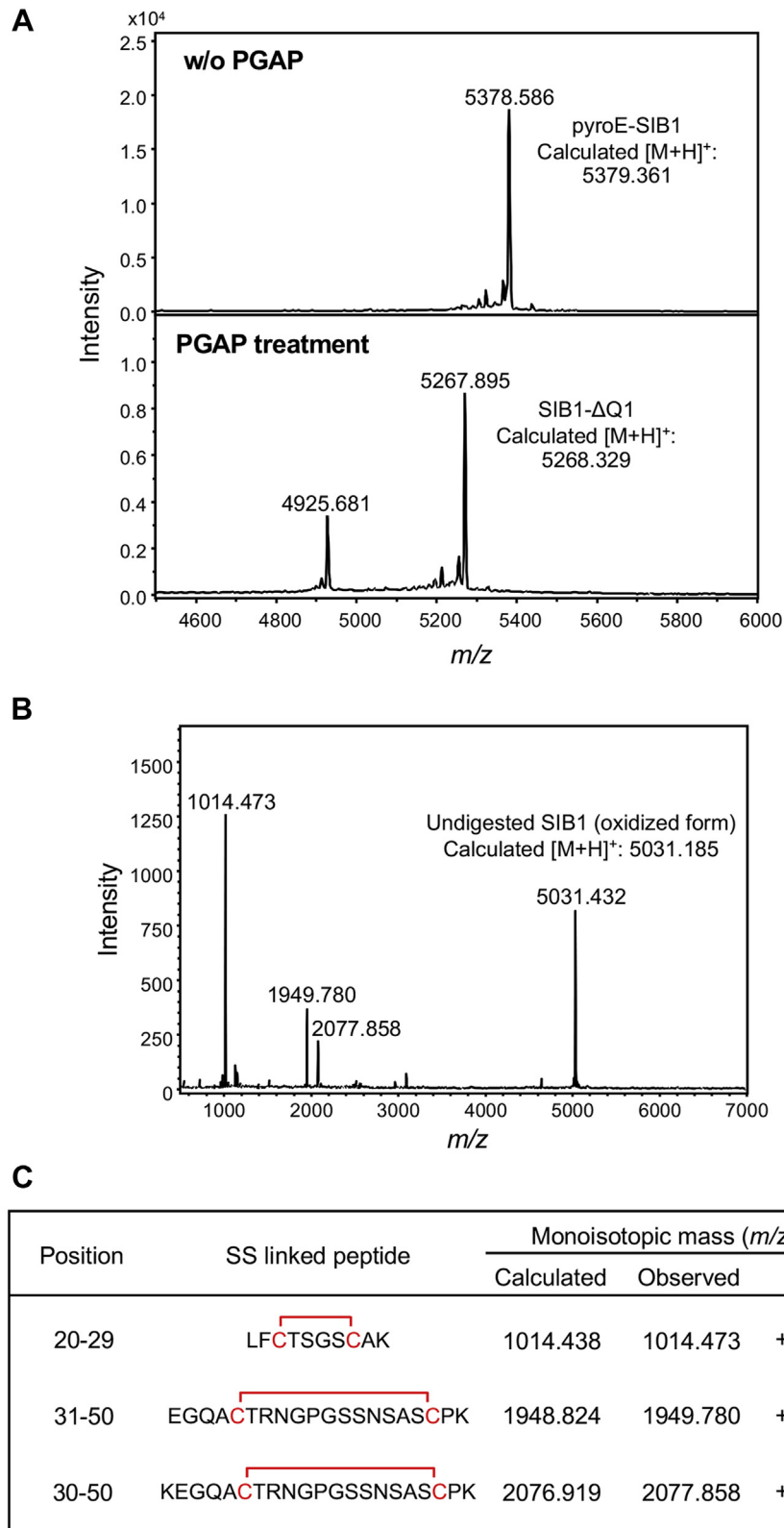


**Figure 4. Post-transcriptional modification analyses of SIB1.** A, confirmation of pyroglutamylation of SIB1. Pyroglutamate aminopeptidase (PGAP)-untreated (*upper panel*) and PGAP-treated (*lower panel*) SIB1 were analyzed using MALDI-TOF-MS. B, determination of disulfide linkages of SIB1. SIB1 after Lys-C treatment was analyzed using MALDI-TOF-MS. C, the assignments of SS-linked peptides of SIB1 obtained by Lys-C digestion. SIB, Suppression of Immunity in *N. benthamiana*.

## Effector with unique structure suppresses plant immunity

**Table 1**  
Statistics of the NMR structure calculation<sup>a</sup>

Total number of NOEs	566
Short range, $ i - j  \leq 1$	305
Medium range, $1 <  i - j  < 5$	59
Long range, $ i - j  \geq 5$	202
Angle constraints ( $\phi$ , $\psi$ )	23, 23
Hydrogen bonds (pair)	16
Disulfide bonds (pair)	3
RMSD for residues 2–49 (Å)	
Average backbone RMSD to mean	0.59 ± 0.09
Average heavy atom RMSD to mean	1.37 ± 0.15
Ramachandran plot (%)	
Most favored region	70.8 ± 3.49
Additionally allowed region	21.8 ± 4.05
Generously allowed region	5.39 ± 3.07
Disallowed region	2.31 ± 2.23

<sup>a</sup> The NMR structure was calculated using XPLOR-NIH, version 3.3. No violation was observed in both distance (>0.5 Å) and dihedral angle (>5°) constraints.

pathogens such as the oomycete pathogen *P. infestans* (39–41). SIB1 also partially suppressed INF1-induced cell death in *N. benthamiana*. It has been reported that the silencing of *Rboh* genes leads to a reduction and delay in HR cell death caused by INF1 in *N. benthamiana* (41). Therefore, SIB1-mediated suppression of the ROS burst may be involved in the SIB1-mediated suppression of INF1-induced cell death. On the other hand, *NbRbohB* silencing decreases resistance to *P. infestans* but not to *C. orbiculare* (39). Therefore, the increased susceptibility of *N. benthamiana* to *C. orbiculare* via transient expression of SIB1 is unlikely to depend on the SIB1-mediated suppression of the ROS burst. SIB1 may be able to suppress other immune responses in addition to the ROS burst.

In the case of *C. orbiculare* inoculation on *N. benthamiana*, RT-qPCR analysis suggested that the expression of *SIB1* was highest at 12 hpi, when the pathogen has already developed appressoria for host invasion, and was strongly reduced at 72 hpi. This result suggests that SIB1 may contribute to the primary stage of host invasion. By contrast, in the case of *C. orbiculare* inoculation on cucumber, the expression of *SIB1* was highest at 48 hpi, and its expression level remained high at 72 hpi. These findings suggest that *C. orbiculare* changes the expression pattern of effector genes, including *SIB1*, during infection of two unrelated susceptible plants, cucumber and *N. benthamiana*. In addition, the inoculation assays using the *SIB1*-knockout mutants revealed that *SIB1* was not essential for the virulence of *C. orbiculare* on *N. benthamiana*, cucumber, and melon, although the transient expression of SIB1 in *N. benthamiana* increased the susceptibility to *C. orbiculare*. We now consider that other effectors of *C. orbiculare* may have functional redundancy with SIB1.

The three-dimensional structure of SIB1 comprises five  $\beta$ -strands each with three disulfide bonds. A pair of  $\beta$ -strands forms a parallel  $\beta$ -sheet, and the others are antiparallel. We tried homology searches to find proteins with SIB1-like topology. A search of SAS (<http://www.ebi.ac.uk/thornton-srv/databases/sas/>) and 3D-BLAST (<http://3dblast.life.nctu.edu.tw/>) found no similar structures in these databases. We also tried ProFunc (<http://www.ebi.ac.uk/thornton-srv/databases/cgi-bin/profunc>), and the survey suggested two antifungal

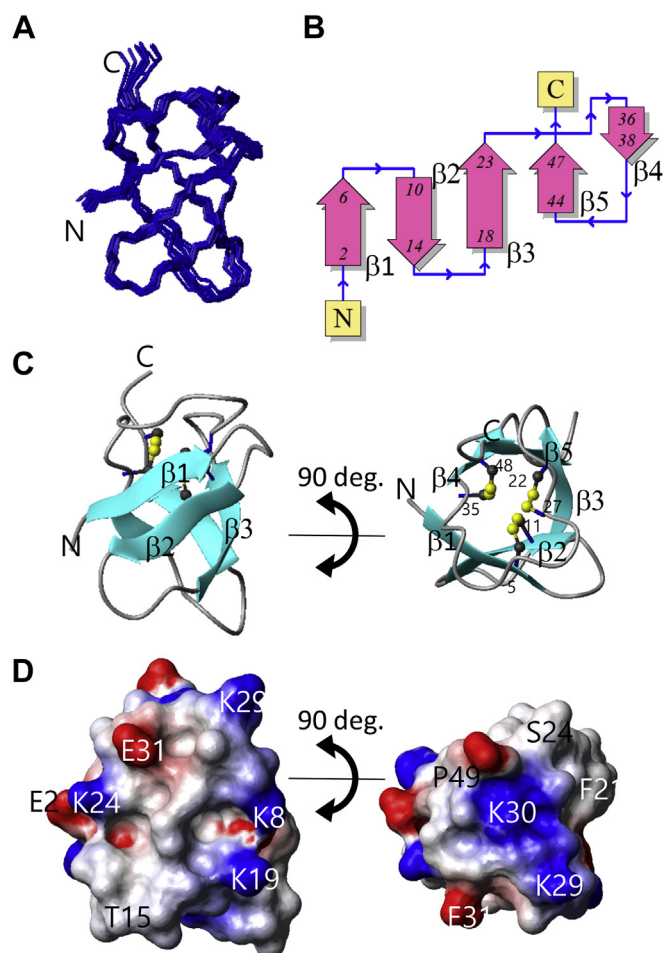


**Figure 5. Three-dimensional structure of SIB1.** Overlay of 20 NMR structures (A), topology of five  $\beta$ -strands (B), ribbon model of the representative structure using a ball-and-stick representation of the three disulfide bonds (C), and molecular surface charge distribution (D). B, generated on the Protein Data Bank sum Web site (<http://www.ebi.ac.uk/thornton-srv/databases/cgi-bin/pdbsum/GetPage.pl?pdbcode=index.html>). The molecular surface shown in D is colored red (negative), blue (positive), and white (hydrophobic). SIB, Suppression of Immunity in *N. benthamiana*.

proteins comprising five  $\beta$ -strands (PDB codes: 2KCN and 1AFP) as the structural neighbors, but both of them show all antiparallel  $\beta$ -barrel topology. In both structures, there are intramolecular disulfide bonds like SIB1. It is thought that the disulfide bonds fundamentally determine their high stability (42, 43). Thus, the intramolecular disulfide bonds found in SIB1 would also contribute to its stability.

Interestingly, both the two peptides found as the structural neighbors of SIB1 display antifungal activity. For their biological activities, they share common structural features on their molecular surfaces. Each has a positively charged area composed of several Lys residues and a hydrophobic area formed by several Tyr residues (42, 43). Both areas are expected to be necessary for their function; the cationic site binds to the anionic part of membrane phospholipids, and the hydrophobic site binds to the hydrophobic moiety of phospholipids. Although SIB1 also has a Lys-rich region on the surface as shown in Figure 5D, the SIB1 surface does not have a Tyr cluster because of no Tyr residue. Thus, distinct



structural characteristics of SIB1 should be related to its functional mechanism to be uncovered.

We observed pyroglutamylation of SIB1 at the N terminus in the present study. Similar N-terminal modification has been reported for many peptides and proteins. For example, brazzein, a sweet-tasting protein of African plants that adopts a well-known protein fold seen in defensins and arthropod toxins, has a pyroglutamylated N-terminal end (44). This modification may be necessary for preventing protein degradation in host cells (45). Therefore, it is possible that the N-terminal modification of SIB1 occurs in nature and functions to extend its lifetime in plant cells. For further understanding of the molecular function of the effector SIB1, especially in the suppression of immunity in *N. benthamiana*, further studies are needed for the comprehensive mutational analyses of SIB1 based on the unraveled SIB1 structure and identification of the *N. benthamiana* proteins targeted by SIB1.

## Experimental procedures

### Fungal strains and culture condition

*C. orbiculare* strain 104-T (MAFF240422) (stock culture of the Laboratory of Plant Pathology, Kyoto University) was used as the wildtype strain. For targeted gene disruption of *SIB1*, we generated the *lig4* $\Delta$  strain from 104-T and used this strain as the parental strain in this study. All fungal strains were maintained on PDA medium (3.9% [w/v] PDA; Nissui) at 24 °C in the dark.

### Plasmid constructions

To express candidate genes in plants, pBICP35-CE1-CE8 transient expression vectors under the control of the 35S promoter were constructed using an In-Fusion system (Clontech, TaKaRa). The fragment containing the complementary DNA of CE1 was amplified with the primers 35S\_CE1\_Fw and 35S\_CE1\_Rv. The fragment was contained in a BamHI site and introduced into the BamHI site of pBICP35, producing pBICP35-CE1. The other candidate gene plasmids used for transient expression were constructed in a similar way as pBICP35-CE1. pBICP35-SIB1-HA was also generated from pBICP35-CE7 by using primers 35S\_SIB1\_Fw and 35S\_SIB1-HA\_Rv. To generate the plasmid pBICP35-GFP-HA, the GFP fragment was amplified with primers 35S\_eGFP\_Fw and 35S\_eGFP-HA\_Rv. This fragment containing a BamHI site was introduced into the BamHI site of pBICP35. The plasmid pBIC35-MoNIS1-HA and the plasmid pBICP35-INF1 used in this study were constructed previously (16).

To delete *LIG4* of *C. orbiculare* (GenBank accession number: TDZ18841), we first generated pBATTEFPGEN. The geneticin-resistant gene cassette was amplified from pII99 (46) with the primers GENAS1B and GENS1X, and the amplified fragment was digested with XbaI and BamHI, and then introduced into pBATTEFP (47), resulting in pBATTEFPGEN. The 5'-upstream region of *LIG4* in *C. orbiculare* was amplified using genomic PCR with the primers CoLIG5SN2 and CoLIG5ASN2. The fragment was digested with NotI and

introduced into pBATTEFPGEN, resulting in pBATTEFPGEN5L. The 3'-downstream region *LIG4* was amplified with the primers CoLIG3SA5 and CoLIG3ASA5. The fragment was digested with ApaI and introduced into pBATTEFPGEN5L, resulting in pBATTEFPGENLIG4KO.

To delete *SIB1* of *C. orbiculare*, we constructed a gene-disruption vector, pCB1636SIB1, using the two-step In-Fusion strategy (Clontech, TaKaRa). First, the ~2.0-kb upstream region of *SIB1* was amplified using PCR with the primers SIB1\_Up\_Fw and SIB1\_Up\_Rv, and the fragment was digested with ApaI. This fragment was then introduced into the ApaI-digested pCB1636 (48), resulting in pCB1636S5. Second, the ~2.0-kb downstream region of *SIB1* was amplified using PCR with the primers SIB1\_Down\_Fw and SIB1\_Down\_Rv, and the fragment was digested with EcoRI. This fragment was introduced into the EcoRI-digested pCB1636S5, resulting in pCB1636SIB1. The primers used for plasmid construction are listed in Table S2.

To produce SIB1 protein in tobacco BY-2 cells, we designed the amino acid sequence for the SIB1 protein fused with an extracellular signal peptide of *Arabidopsis* chitinase (SPSIB1). Next, artificial *SP-SIB1* was synthesized by optimizing the codons in tobacco and introducing restriction enzyme sites for cloning at both ends (IDT; Table S2). The artificial *SP-SIB1* was introduced into a chemically inducible ToMV vector (pBICLBSER-ToMV) (28). The resultant plasmid was named pBICLBSERToMV-SP-SIB1.

### RNA isolation and RNA-Seq

RNA was isolated as previously described (5). In brief, total RNA from conidia containing 3-day-old hyphae grown in potato dextrose broth at 25 °C and infected *N. benthamiana* leaves at dpi 1, 3, and 7 were isolated using a Plant RNeasy Mini kit with DNase I treatment (Qiagen). Three biological replicates were prepared for each tissue type. Unstranded RNA-Seq libraries were prepared from poly(A)+-tailed RNA using a TruSeq Sample Prep kit according to the manufacturer's instructions before sequencing on an Illumina HiSeq 2000 sequencer to 50 bp in single-read mode. Reads were mapped to the *C. orbiculare* genome (version 2 accession number, AMCV02000000) using STAR, version 2.6.0a (49) with the setting `-alignIntronMax 1000`. Read counts were obtained using Rsubread (version 1.32.2) (50) using the following settings: `isGTFAnnotationFile = TRUE`, `GTF.featureType = "exon"`, `GTF.attrType = "Parent"`. Reads per kilobase million values (51) were calculated using edgeR (52) after applying `calcNormFactors`.

### Agrobacterium tumefaciens-mediated transient expression assay in *N. benthamiana*

For the agroinfiltration assay, *N. benthamiana* plants (5–6 weeks old) were used. Plants were grown in a controlled environment chamber at 25 °C with 16 h of illumination per day. Each construct was transformed into *A. tumefaciens* strain GV3101 by electroporation. Each *Agrobacterium* was cultured in Luria-Bertani medium broth containing

## Effector with unique structure suppresses plant immunity

kanamycin (50 µg/ml), rifampicin (50 µg/ml), and gentamicin (50 µg/ml). The cells were harvested by centrifugation and then resuspended in MMA induction buffer (1 l of MMA: 5 g of Murashige and Skoog salts, 1.95 g of MES, 20 g of sucrose, and 200 µM acetosyringone, pH 5.6). All suspensions (absorbance of 0.3 at 600 nm) of the *Agrobacterium* strains were incubated for 1 h before being infiltrated into *N. benthamiana* leaves using a needleless syringe.

### Virulence-enhancement assay

*N. benthamiana* leaves were infiltrated with each *A. tumefaciens*. The infiltrated leaves were incubated for 2 days, after which 10 µl of conidial suspensions ( $5 \times 10^5$  conidia/ml) of the *C. orbiculare* wildtype strain were drop-inoculated onto the infiltration areas of detached *N. benthamiana* leaves. Inoculated leaves were incubated at 24 °C for 5 days. Quantitative assessment of lesion development was obtained using ImageJ software (<https://imagej.nih.gov/ij/>) for three biological replicates.

### Suppression assay of INF1-induced cell death

Each tested gene was expressed in the *A. tumefaciens*-mediated transient expression assay as mentioned previously. At 1 day after the first agroinfiltration, the second agroinfiltration with recombinant *A. tumefaciens* carrying p35S-INF1 was performed at same infiltration site. All suspensions (absorbance of 0.3 at 600 nm) of the *Agrobacterium* strains were incubated for 1 h before infiltration. The suspensions were infiltrated into *N. benthamiana* leaves using a needleless syringe. INF1-induced lesions were observed at 3 to 5 days after the second infiltration.

### ROS assay

ROS production was monitored using a luminol-based assay (53). Leaf discs were made using a circular borer (diameter of 5 mm), and the collected leaf discs were incubated overnight in distilled water. For measurement of ROS production, leaf discs were placed in a 96-well plate containing 50 µl of distilled water and 50 µl of assay solution containing 400 µM luminol (FUJIFILM Wako Pure Chemical Corporation; 127-02581), 20 µg/ml peroxidase (Sigma-Aldrich; P6782), and either 400 µg/ml chitin (Sigma-Aldrich; C9752) or 2 µM flg22 (Invitrogen) were added to the wells. Luminescence was measured using a Luminoskan Ascent 2.1 (Thermo Fisher Scientific).

### RT-qPCR analysis of SIB1 expression

Cucumber cotyledons were drop-inoculated with conidial suspension ( $1 \times 10^6$  conidia/ml) of the *C. orbiculare* wildtype strain covering as much as possible of the abaxial surface. After incubation for 0, 4, 8, 12, 24, 48, and 72 h, the inoculated epidermis containing the fungal cells was peeled off from three cotyledons for each sample and immediately frozen in liquid nitrogen to fix the gene expression profile. As for the preparation of 0 h samples, once conidial suspensions were inoculated, inoculated epidermis were immediately peeled off. As for

inoculation on *N. benthamiana*, leaves were spray-inoculated with conidial suspension ( $1 \times 10^6$  conidia/ml) of the *C. orbiculare* wildtype strain. Then the whole leaves were frozen at particular time point in liquid nitrogen to fix gene expression profiles, one leaf for each sample. The frozen tissues were ground, and total RNA was extracted by using the Agilent Plant RNA Isolation Mini Kit (Agilent Technologies). Three biological replicates were prepared for each time point. The relative gene expression of *SIB1* was assessed by RT-qPCR using primers SIB1\_qRT\_F and SIB1\_qRT\_R (Table S2). The TB Green Premix Ex Taq (TaKaRa) was used with a Thermal Cycler Dice Real Time System TP800 (TaKaRa) for RT-qPCR. The relative expression levels were normalized against the *C. orbiculare* actin gene (GenBank accession number: AB778553.1).

### Transformation of BY-2 cells

Tobacco BY-2 cells were grown in Linsmaier and Skoog medium supplemented with 3% sucrose and 0.2 mg/l 2,4-dichlorophenoxyacetic acid at 26 °C (54). To generate the *SPSIB1*-expressing transgenic line, pBICHgLBSXVE expressing the artificial transcription factor XVE, which activates transcription by binding with 17β-estradiol (28), and pBICLBSER-ToMV-SP-SIB1 were introduced into tobacco BY-2 cells using the *Agrobacterium* method (55). Transgenic lines were selected on agar medium containing the appropriate selective agents, 50 mg/l hygromycin, 100 mg/l kanamycin, and 500 mg/l carbenicillin. Suspended cells developed from calli were grown in 3 ml of liquid medium in 6-well culture plates during the primary screening, after which they were transferred to 150 ml of liquid medium in 500-ml flasks with constant shaking at 135 rpm. After the initial culture for 2 to 3 weeks, the suspension cells were maintained without selective agents. These cell lines were suspension cultured in normal MS medium and MS medium labeled with an  $^{15}\text{N}$  nitrogen source for NMR analysis.

### Protein production and purification

Protein production was induced by adding 10 µM 17β-estradiol (28). After 4 days, SIB1 protein had accumulated in the culture medium, and the culture medium was collected by centrifugation. For the first purification, the ammonium sulfate precipitation method was performed, and the protein in the 60% ammonium sulfate supernatant was mostly SIB1 protein. The solvent of the supernatant was replaced with phosphate buffer (pH 6.8) by dialysis. Next, the supernatant was purified by gel filtration chromatography using AKTA prime plus (GE Healthcare) to obtain a single protein. For the gel filtration chromatography purification, a Superdex 75 10/300GL column (Amersham Biosciences) was used, and the buffer was phosphate buffer (pH 6.8) at a flow rate of 0.1 ml min<sup>-1</sup> at room temperature. Elution was monitored by absorbance at 280 nm. The collected fraction was concentrated using a centrifugal concentrator (CC-105; Tomy Seiko, Inc) and then used for NMR analysis.

### Gene disruption in *C. orbiculare*

To delete *SIB1*, we first generated the *lig4* $\Delta$  strain from 104-T, in which the homologous recombination ratio is expected to be increased, because DNA ligase 4 (Lig4) is reported to be a key molecule in the nonhomologous end-joining pathway (24). To generate the *lig4*-knockout strain, we introduced pBATTEFPGENLIG4KO into protoplasts of *C. orbiculare* 104-T. Preparation of protoplasts and transformation of *C. orbiculare* were performed according to a method described previously (56). We first selected geneticin-resistant transformants, and the bialaphos-sensitive transformants were selected from the geneticin-resistant transformants. The selected bialaphos-sensitive transformants were subjected to genomic PCR analysis using the primers Co5-Jcheck3 and J-check-CoLIG3AS to check the disruption of *LIG4*. The *lig4* $\Delta$  strains obtained exhibited colony growth, conidiation, and virulence on cucurbits to the same extent as the parental wildtype strain 104-T. To generate *SIB1*-knockout mutants, we introduced the gene-disruption vector pCB1636SIB1 into protoplasts of the *C. orbiculare lig4* $\Delta$  strain (generated in the 104-T background as described previously). We selected hygromycin-resistant transformants. Transformants were then analyzed by genomic PCR with the primers SIB1\_col\_F and SIB1\_col\_R. Hygromycin-resistant, geneticin-resistant, and bialaphos-sensitive transformants were selected in regeneration medium containing hygromycin B (100  $\mu\text{g}/\text{ml}$ ), geneticin (200  $\mu\text{g}/\text{ml}$ ), and bialaphos (25  $\mu\text{g}/\text{ml}$ ), respectively.

### Inoculation of *N. benthamiana*, cucumber, and melon

Conidial suspensions collected from the 7-day-old colony of each strain formed on PDA were drop-inoculated onto detached *N. benthamiana* leaves and cotyledons of cucumber and melon; the volume was 10  $\mu\text{l}$  for each drop. All conidial suspensions were used at a concentration of  $5 \times 10^5$  conidia/ml. In *N. benthamiana*, the leaves were collected from 5- to 6-week-old plants. The cotyledons of cucumber and melon were derived from 10-day-old plants. The phenotype of lesions developed was observed after incubation for 7 days at 24  $^{\circ}\text{C}$ .

### MS analyses

Samples with 0.1% TFA were filtered through a 0.45- $\mu\text{m}$  filter, and the filtrates were injected directly into a C18 column (4.6 mm inner diameter  $\times$  250 mm, Protein-R; Nacalai Tesque) equilibrated with 100% mobile phase A (0.1% TFA in water). Samples were separated with a linear gradient from 0% to 50% mobile phase B (0.1% TFA in acetonitrile) in 40 min at a 0.5-ml/min flow rate. The eluate was monitored at 220 nm, and the fraction including SIB1 was verified by MALDI-TOF-MS (ultrafleXtreme; Bruker). The peptide concentration was estimated using a bicinchoninic acid protein assay reagent kit (Thermo Fisher Scientific).

To confirm the pyroglutamylation of SIB1, 5  $\mu\text{g}$  (1  $\mu\text{g}/\mu\text{l}$ ) of SIB1 dissolved in buffer (6 M urea and 0.1 M triethylamine bicarbonate [TEAB]) was incubated for reduction with 2 mM

Tris(2-carboxyethyl)phosphine for 30 min at 37  $^{\circ}\text{C}$  followed by alkylation with 55 mM iodoacetamide (IAA) in the dark for 30 min at room temperature. The sample solution was acidified with 10% TFA and desalted using SDB-Stage Tip (57). The desalted sample was dried under vacuum and dissolved in buffer (50 mM  $\text{Na}_2\text{PO}_4$ , pH 7.0, 10 mM dithiothreitol, and 1 mM ethylenediaminetetraacetic acid), and 10  $\mu\text{l}$  (1 mU) of *Pfu* PGAP (TaKaRa) was added. After incubation for 5 h at 50  $^{\circ}\text{C}$ , the sample was acidified with 10% TFA, desalted using SDB-Stage Tip, and dried under vacuum. The PGAP-treated sample was analyzed using MALDI-TOF-MS. The Unimod database (<http://www.unimod.org>) was used to analyze the post-transcriptional modification.

To examine whether Cys residues of SIB1 were in the oxidized form, 15  $\mu\text{g}$  (1  $\mu\text{g}/\mu\text{l}$ ) of SIB1 dissolved in buffer (6 M urea and 0.1 M TEAB) was used as the stock solution. Using this stock, three samples at different conditions were prepared: (i) untreated, (ii) alkylated with 55 mM IAA under nonreducing conditions, and (iii) reduced with 2 mM Tris(2-carboxyethyl)phosphine and alkylated with 55 mM IAA. All three samples were acidified with 10% TFA and desalted using SDB-Stage Tip. The desalted sample was dried under vacuum and analyzed using MALDI-TOF-MS. To identify the disulfide linkages, we used the method reported previously (58). In brief, SIB1 (5  $\mu\text{g}$ , 1  $\mu\text{g}/\mu\text{l}$ ) was dissolved in buffer (6 M urea and 0.1 M TEAB), and Lys-C was added to the sample at a 1:100 ratio of Lys-C. After overnight digestion at 37  $^{\circ}\text{C}$  under nonreducing conditions, the sample solution was acidified with 10% TFA and desalted using SDB-Stage Tip. The desalted solution was dried under vacuum and analyzed using MALDI-TOF-MS. The assignment of peaks derived from peptides with disulfide linkages was performed using BioTools (Bruker Daltonics).

### NMR study of SIB1

$^{15}\text{N}$ -labeling of SIB1 using the BY-2 system was prepared using the method reported previously (27, 29, 30), and the sample was purified as described previously. The  $^{15}\text{N}$ -labeled NMR sample was prepared at a concentration of 0.8 mM dissolved in water containing 10% deuterium oxide and 100 mM KCl. The sample pH was adjusted to 6.3 by direct reading with a pH meter. All NMR data were recorded on a Bruker AVANCE III 800 equipped with a TCI cryogenic probe. The sample temperature during the NMR experiments was kept at 25.0  $^{\circ}\text{C}$ .

To determine the structure,  $^1\text{H}$ - $^{15}\text{N}$  heteronuclear single quantum coherence (59, 60),  $^{15}\text{N}$ -edited NOESY (61),  $^{15}\text{N}$ -edited TOCSY (62), NOESY (63) and TOCSY (64) were observed. The NOE mixing time and TOCSY spin-lock time were set as 100 and 70 ms, respectively. In addition, heteronuclear  $\{^1\text{H}\}$ - $^{15}\text{N}$  NOE experiments (65) were performed to provide information about the internal protein dynamics. Water suppression in the NMR experiments was achieved using WATERGATE (66) or a water flip-back pulse (67). All free induction decay data were processed using NMRPipe (68) and analyzed on Sparky (<http://www.cgl.ucsf.edu/home/>)

## Effector with unique structure suppresses plant immunity

sparky). The distance constraints were obtained from NOE peaks. The angle constraints were obtained using TALOS+ (69) analysis using  $^1\text{HN}$ ,  $^{15}\text{N}$ , and  $^1\text{H}$  chemical shifts. Preliminary 50 structures of SIB1 were calculated with CYANA 2.1 (33) and PONDEROSA-C/S (34). Then, the preliminary structures were subjected to calculate the refined structures in explicit water by using ARIA 2.2 (35) and XPLOR-NIH 3.3 (36). The final ten structures with lower energy term and without violation for both NOE ( $>0.5 \text{ \AA}$ ) and dihedral ( $>5^\circ$ ) restraints were selected from the refined structures. The structural figures were generated using MOLMOL (70) or PyMOL (71).

The pulse sequences used to study protein dynamics have been published (72). In our study, the  $T_1$  relaxation analysis used a series of ten experiments with inversion recovery delays set at 75, 100, 150, 200, 250, 300, 400, 500, 700, and 950 ms. Similar to the  $T_1$  experiments,  $T_2$  measurements were also performed as a series of ten experiments with different Carr–Purcell–Meiboom–Gill delays of 25, 60, 80, 120, 150, 200, 300, 400, 500, and 750 ms. The  $T_1$  and  $T_2$  values were estimated by fitting the peak volume,  $I$ , using the equation,  $I = I_0 \exp(-t/T_{1,2})$ . As for the heteronuclear NOE experiments, a recycle delay of 5 s was used after each scan. The NOE values were obtained by calculating the ratio of the peak intensity recorded with the saturation of protons divided by the peak intensity recorded without saturation.

### Data availability

Protein structure coordinate data are available at PDB (<https://www.rcsb.org/>). Accession codes for the structural coordinates and chemical shifts deposited in the PDB and Biological Magnetic Resonance Data Bank are 7EAU and 36412, respectively. RNA-Seq data are accessible in Gene Expression Omnibus database of the National Center for Biotechnology Information under Gene Expression Omnibus Series accession number GSE178879.

**Supporting information**—This article contains supporting information.

**Acknowledgments**—We thank all the technicians working at Center for Nano Materials and Technology, Japan Advanced Institute of Science and Technology, for maintenance of instruments used in this work. We also thank Akiko Mizuno and Hiroko Hayashi in Ishikawa Prefectural University and Fumika Takahashi in Kyoto University for excellent technical assistance as well as Manaka Iino for his contribution to a part of the NMR data analyses.

**Author contributions**—M. M., S. O., and Y. T. conceptualization; M. M. methodology; J.-I. K. formal analysis; R. Z., N. I., M. M., R. O., S. S.-O., T. I., and S. O. investigation; P. G. and K. S. resources; R. Z., P. G., and K. S. data curation; R. Z., M. M., S. O., and Y. T. writing—original draft; S. O. and Y. T. writing—review and editing; Y. T. supervision; P. G., K. S., S. O., and Y. T. funding acquisition.

**Funding and additional information**—This work was supported by Grants-in-Aid for Scientific Research (18H02204 and 21H05032 [to

Y. T.], 17K08194 [to S. O.], 17H06172 [to K. S.], 19K15846 [to P. G.] [KAKENHI]).

**Conflict of interest**—The authors declare that they have no conflicts of interest with the contents of this article.

**Abbreviations**—The abbreviations used are: BY-2, *Nicotiana tabacum* cv. Bright Yellow 2; dpi, days post inoculation; eGFP, enhanced GFP; hpi, hours post inoculation; HR, hypersensitive response; IAA, iodoacetamide; PAMP, pathogen-associated molecular pattern; PCD, programmed cell death; PDA, potato dextrose agar; PDB, Protein Data Bank; PGAP, pyroglutamate aminopeptidase; PTI, pathogen-associated molecular pattern–triggered immunity; qPCR, quantitative PCR; RBOH, respiratory burst oxidase homolog; ROS, reactive oxygen species; SIB, Suppression of Immunity in *N.ben-thamiana*; TEAB, triethylamine bicarbonate; ToMV, tobamovirus.

### References

1. Chisholm, S. T., Coaker, G., Day, B., and Staskawicz, B. J. (2006) Host-microbe interactions: Shaping the evolution of the plant immune response. *Cell* **124**, 803–814
2. Jones, J. D., and Dangl, J. L. (2006) The plant immune system. *Nature* **444**, 323–329
3. Win, J., Chaparro-Garcia, A., Belhaj, K., Saunders, D. G., Yoshida, K., Dong, S., Schornack, S., Zipfel, C., Robatzek, S., Hogenhout, S. A., and Kamoun, S. (2012) Effector biology of plant-associated organisms: Concepts and perspectives. *Cold Spring Harb. Symp. Quant. Biol.* **77**, 235–247
4. Cui, H., Tsuda, K., and Parker, J. E. (2015) Effector-triggered immunity: From pathogen perception to robust defense. *Annu. Rev. Plant Biol.* **66**, 487–511
5. Gan, P., Ikeda, K., Irieda, H., Narusaka, M., O’Connell, R. J., Narusaka, Y., Takano, Y., Kubo, Y., and Shirasu, K. (2013) Comparative genomic and transcriptomic analyses reveal the hemibiotrophic stage shift of *Colletotrichum* fungi. *New Phytol.* **197**, 1236–1249
6. O’Connell, R. J., Thon, M. R., Hacquard, S., Amyotte, S. G., Kleemann, J., Torres, M. F., Damm, U., Buiate, E. A., Epstein, L., Alkan, N., Altmüller, J., Alvarado-Balderrama, L., Bauser, C. A., Becker, C., Birren, B. W., et al. (2012) Lifestyle transitions in plant pathogenic *Colletotrichum* fungi deciphered by genome and transcriptome analyses. *Nat. Genet.* **44**, 1060–1065
7. Perfect, S. E., Hughes, H. B., O’Connell, R. J., and Green, J. R. (1999) *Colletotrichum*: A model genus for studies on pathology and fungal-plant interactions. *Fungal Genet. Biol.* **27**, 186–198
8. Kubo, Y., Nakamura, H., Kobayashi, K., Okuno, T., and Furusawa, I. (1991) Cloning of a melanin biosynthetic gene essential for appressorial penetration of *Colletotrichum lagenarium*. *Mol. Plant Microbe Interact.* **4**, 440–445
9. Kubo, Y., and Takano, Y. (2013) Dynamics of infection-related morphogenesis and pathogenesis in *Colletotrichum orbiculare*. *J. Gen. Plant Pathol.* **79**, 233–242
10. Cannon, P. F., Damm, U., Johnston, P. R., and Weir, B. S. (2012) *Colletotrichum* - current status and future directions. *Stud. Mycol.* **73**, 181–213
11. Liu, B., Wasilwa, L. A., Morelock, T. E., O’Neill, N. R., and Correll, J. C. (2007) Comparison of *Colletotrichum orbiculare* and several allied *Colletotrichum* spp. for mtDNA RFLPs, intron RFLP and sequence variation, vegetative compatibility, and host specificity. *Phytopathology* **97**, 1305–1314
12. Goodin, M. M., Zaitlin, D., Naidu, R. A., and Lommel, S. A. (2008) *Nicotiana benthamiana*: Its history and future as a model for plant-pathogen interactions. *Mol. Plant Microbe Interact.* **21**, 1015–1026
13. Shen, S., Goodwin, P. H., and Hsiang, T. (2001) Infection of *Nicotiana* species by the anthracnose fungus, *Colletotrichum orbiculare*. *Eur. J. Plant Pathol.* **107**, 767–773

14. Takano, Y., Takayanagi, N., Hori, H., Ikeuchi, Y., Suzuki, T., Kimura, A., and Okuno, T. (2006) A gene involved in modifying transfer RNA is required for fungal pathogenicity and stress tolerance of *Colletotrichum lagenarium*. *Mol. Microbiol.* **60**, 81–92
15. Irieda, H., Maeda, H., Akiyama, K., Hagiwara, A., Saitoh, H., Uemura, A., Terauchi, R., and Takano, Y. (2014) *Colletotrichum orbiculare* secretes virulence effectors to a biotrophic interface at the primary hyphal neck via exocytosis coupled with SEC22-mediated traffic. *Plant Cell* **26**, 2265–2281
16. Yoshino, K., Irieda, H., Sugimoto, F., Yoshioka, H., Okuno, T., and Takano, Y. (2012) Cell death of *Nicotiana benthamiana* is induced by secreted protein NIS1 of *Colletotrichum orbiculare* and is suppressed by a homologue of CgDN3. *Mol. Plant Microbe Interact.* **25**, 625–636
17. Isozumi, N., Inoue, Y., Imamura, T., Mori, M., Takano, Y., and Ohki, S. (2019) Ca<sup>2+</sup>-dependent interaction between calmodulin and CoDN3, an effector of *Colletotrichum orbiculare*. *Biochem. Biophys. Res. Commun.* **514**, 803–808
18. Irieda, H., Inoue, Y., Mori, M., Yamada, K., Oshikawa, Y., Saitoh, H., Uemura, A., Terauchi, R., Kitakura, S., Kosaka, A., Singkaravanit-Ogawa, S., and Takano, Y. (2019) Conserved fungal effector suppresses PAMP-triggered immunity by targeting plant immune kinases. *Proc. Natl. Acad. Sci. U. S. A.* **116**, 496–505
19. Shimada, C., Lipka, V., O'Connell, R., Okuno, T., Schulze-Lefert, P., and Takano, Y. (2006) Nonhost resistance in *Arabidopsis-colletotrichum* interactions acts at the cell periphery and requires actin filament function. *Mol. Plant Microbe Interact.* **19**, 270–279
20. Inagaki, A., Takano, Y., Kubo, Y., Mise, K., and Furusawa, I. (2000) Construction of an equalized cDNA library from *Colletotrichum lagenarium* and its application to the isolation of differentially expressed genes. *Can. J. Microbiol.* **46**, 150–158
21. Armenteros, J. J. A., Tsirigos, K. D., Sonderby, C. K., Petersen, T. N., Winther, O., Brunak, S., von Heijne, G., and Nielsen, H. (2019) SignalP 5.0 improves signal peptide predictions using deep neural networks. *Nat. Biotechnol.* **37**, 420–423
22. Ramachandran, S. R., Yin, C. T., Kud, J., Tanaka, K., Mahoney, A. K., Xiao, F. M., and Hulbert, S. H. (2017) Effectors from wheat rust fungi suppress multiple plant defense responses. *Phytopathology* **107**, 75–83
23. Kanneganti, T. D., Huitema, E., Kahir, C., and Kamoun, S. (2006) Synergistic interactions of the plant cell death pathways induced by *Phytophthora infestans* Nep1-like protein PiNPP1.1 and INF1 elicitor. *Mol. Plant Microbe Interact.* **19**, 854–863
24. Ninomiya, Y., Suzuki, K., Ishii, C., and Inoue, H. (2004) Highly efficient gene replacements in *Neurospora* strains deficient for nonhomologous end-joining. *Proc. Natl. Acad. Sci. U. S. A.* **101**, 12248–12253
25. Dohi, K., and Mori, M. (2007) Expression of active enzymes from an inducible tomato-mosaic-virus-based vector in cultured transgenic tobacco BY-2 cells. *Plant Biotechnol.* **24**, 367–373
26. Dohi, K., Nishikiori, M., Tamai, A., Ishikawa, M., Meshi, T., and Mori, M. (2006) Inducible virus-mediated expression of a foreign protein in suspension-cultured plant cells. *Arch. Virol.* **151**, 1075–1084
27. Costa, L. M., Marshall, E., Tesfaye, M., Silverstein, K. A. T., Mori, M., Umetsu, Y., Otterbach, S. L., Papareddy, R., Dickinson, H. G., Boutiller, K., VandenBosch, K. A., Ohki, S., and Gutierrez-Marcos, J. F. (2014) Central cell-derived peptides regulate early embryo patterning in flowering plants. *Science* **344**, 168–172
28. Imamura, T., Isozumi, N., Higashimura, Y., Ohki, S., and Mori, M. (2021) Production of ORF8 protein from SARS-CoV-2 using an inducible virus-mediated expression system in suspension-cultured tobacco BY-2 cells. *Plant Cell Rep.* **40**, 433–436
29. Ohki, S., Dohi, K., Tamai, A., Takeuchi, M., and Mori, M. (2008) Stable-isotope labeling using an inducible viral infection system in suspension-cultured plant cells. *J. Biomol. NMR* **42**, 271–277
30. Ohki, S., Takeuchi, M., and Mori, M. (2011) The NMR structure of stomagen reveals the basis of stomatal density regulation by plant peptide hormones. *Nat. Commun.* **2**, 512
31. Ito, K., Ikemasu, T., and Ishikawa, T. (1992) Cloning and sequencing of the *xynA* gene encoding xylanase A of *Aspergillus kawachii*. *Biosci. Biotechnol. Biochem.* **56**, 906–912
32. Liao, Y. D., Wang, S. C., Leu, Y. J., Wang, C. F., Chang, S. T., Hong, Y. T., Pan, Y. R., and Chen, C. P. (2003) The structural integrity exerted by N-terminal pyroglutamate is crucial for the cytotoxicity of frog ribonuclease from *Rana pipiens*. *Nucleic Acids Res.* **31**, 5247–5255
33. Lopez-Mendez, B., and Guntert, P. (2006) Automated protein structure determination from NMR spectra. *J. Am. Chem. Soc.* **128**, 13112–13122
34. Lee, W., Stark, J. L., and Markley, J. L. (2014) PONDEROSA-C/S: Client-server based software package for automated protein 3D structure determination. *J. Biomol. NMR* **69**, 73–75
35. Rieping, W., Habeck, M., Bardiaux, B., Bernard, A., Malliavin, T. E., and Nilges, M. (2007) ARIA2: Automated NOE assignment and data integration in NMR structure calculation. *Bioinformatics* **23**, 381–382
36. Schwieters, C., Kuszewski, J., Tjandra, N., and Clore, M. (2003) The Xplor-NIH NMR molecular structure determination package. *J. Magn. Reson.* **160**, 65–73
37. Gan, P., Tsushima, A., Narusaka, M., Narusaka, Y., Takano, Y., Kubo, Y., and Shirasu, K. (2019) Genome sequence resources for four phytopathogenic fungi from the *Colletotrichum orbiculare* species complex. *Mol. Plant Microbe Interact.* **32**, 1088–1090
38. Marino, D., Dunand, C., Puppo, A., and Pauly, N. (2012) A burst of plant NADPH oxidases. *Trends Plant Sci.* **17**, 9–15
39. Asai, S., Ohta, K., and Yoshioka, H. (2008) MAPK signaling regulates nitric oxide and NADPH oxidase-dependent oxidative bursts in *Nicotiana benthamiana*. *Plant Cell* **20**, 1390–1406
40. Segonzac, C., Feike, D., Gimenez-Ibanez, S., Hann, D. R., Zipfel, C., and Rathjen, J. P. (2011) Hierarchy and roles of pathogen-associated molecular pattern-induced responses in *Nicotiana benthamiana*. *Plant Physiol.* **156**, 687–699
41. Yoshioka, H., Numata, N., Nakajima, K., Katou, S., Kawakita, K., Rowland, O., Jones, J. D., and Doke, N. (2003) *Nicotiana benthamiana* gp91<sup>phox</sup> homologs *NbrbohA* and *NbrbohB* participate in H<sub>2</sub>O<sub>2</sub> accumulation and resistance to *Phytophthora infestans*. *Plant Cell* **15**, 706–718
42. Campos-Olivas, R., Bruix, M., Santoro, J., Lacadena, J., Martiz del Pozo, A., Gavilanes, J. G., and Rico, M. (1995) NMR solution structure of the antifungal protein from *Aspergillus giganteus*: Evidence for cysteine pairing isomerism. *Biochemistry* **34**, 3009–3021
43. Batta, G., Barna, T., Gaspari, Z., Sandor, S., Kover, K. E., Binder, U., Sarg, B., Kaiserer, L., Chhilar, A. K., Eigentler, A., Leiter, E., Hefedus, N., Pocs, I., Linder, H., and Marx, F. (2009) Functional aspects of the solution structure and dynamics of PAF - a highly-stable antifungal protein from *Penicillium chrysogenum*. *FEBS J.* **276**, 2875–2890
44. Caldwell, J. E., Abildgaard, F., Dzaku, Z., Ming, D., Hellekant, G., and Markley, J. L. (1998) Solution structure of the thermostable sweet-tasting protein brazzein. *Nat. Struct. Mol. Biol.* **5**, 427–431
45. Graciet, E., Walter, F., O'Maoileidigh, D., Pollmann, S., Meyerowitz, E. M., Varshavsky, A., and Wellmer, F. (2009) The N-end rule pathway controls multiple functions during *Arabidopsis* shoot and leaf development. *Proc. Natl. Acad. Sci. U. S. A.* **106**, 13618–13623
46. Namiki, F., Matsunaga, M., Okuda, M., Inoue, I., Nishi, K., Fujita, Y., and Tsuge, T. (2001) Mutation of an arginine biosynthesis gene causes reduced pathogenicity in *Fusarium oxysporum* f. sp. *melonis*. *Mol. Plant Microbe Interact.* **14**, 580–584
47. Asakura, M., Ninomiya, S., Sugimoto, M., Oku, M., Yamashita, S., Okuno, T., Sakai, Y., and Takano, Y. (2009) Atg26-mediated pexophagy is required for host invasion by the plant pathogenic fungus *Colletotrichum orbiculare*. *Plant Cell* **21**, 1291–1304
48. Sweigard, J. A., Chumley, F. G., Carroll, A. M., Farrall, L., and Valent, B. (1997) A series of vectors for fungal transformation. *Fungal Genet. Newsl.* **44**, 52–53
49. Dobin, A., Davis, C. A., Schlesinger, F., Drenkow, J., Zaleski, C., Jha, S., Batut, P., Chaisson, M., and Gingeras, T. R. (2013) Star: Ultrafast universal RNA-seq aligner. *Bioinformatics* **29**, 15–21
50. Liao, Y., Smyth, G. K., and Shi, W. (2019) The R package Rsubread is easier, faster, cheaper and better for alignment and quantification of RNA sequencing reads. *Nucleic Acids Res.* **47**, e47
51. Mortazavi, A., Williams, B. A., McCue, K., Schaeffer, L., and Wold, B. (2008) Mapping and quantifying mammalian transcriptomes by RNA-Seq. *Nat. Methods* **5**, 621–628

## Effector with unique structure suppresses plant immunity

52. Robinson, M. D., McCarthy, D. J., and Smyth, G. K. (2010) edgeR: A bioconductor package for differential expression analysis of digital gene expression data. *Bioinformatics* **26**, 139–140
53. Keppler, L. D., Baker, C. J., and Atkinson, M. M. (1989) Active oxygen production during a bacteria-induced hypersensitive reaction in tobacco suspension cells. *Phytopathology* **79**, 974–978
54. Nagata, T., Nemoto, Y., and Hasezawa, S. (1992) Tobacco BY-2 cell line as the “HeLa” cell in the cell biology of higher plants. *Int. Rev. Cyt.* **132**, 1–30
55. Hagiwara, Y., Komoda, K., Yamanaka, T., Tamai, A., Meshi, T., Funada, R., Tsuchiya, T., Naito, S., and Ishikawa, M. (2003) Subcellular localization of host and viral proteins associated with tobamovirus RNA replication. *EMBO J.* **22**, 344–353
56. Takano, Y., Komeda, K., Kojima, K., and Okuno, T. (2001) Proper regulation of cyclic AMP-dependent protein kinase is required for growth, conidiation, and appressorium function in the anthracnose fungus *Colletotrichum lagenarium*. *Mol. Plant Microbe Interact.* **14**, 1149–1157
57. Rappsilber, J., Mann, M., and Ishihama, Y. (2007) Protocol for micro-purification, enrichment, pre-fractionation and storage of peptides for proteomics using StageTips. *Nat. Protoc.* **2**, 1896–1906
58. Isozumi, N., Masubuchi, Y., Imamura, T., Mori, M., Koga, H., and Ohki, S. (2021) Structure and antimicrobial activity of NCR169, a nodule-specific cysteine-rich peptide of *Medicago truncatula*. *Sci. Rep.* **11**, 9923
59. Bodenhausen, G., and Ruben, D. J. (1980) Natural abundance nitrogen-15 NMR by enhanced heteronuclear spectroscopy. *Chem. Phys. Lett.* **69**, 185–189
60. Kay, L. E., Keifer, P., and Saarienen, T. (1992) Pure absorption gradient enhanced heteronuclear single quantum correlation spectroscopy with improved sensitivity. *J. Am. Chem. Soc.* **114**, 10663–10665
61. Fesik, S., and Zuiderweg, E. R. P. (1988) Heteronuclear three-dimensional NMR spectroscopy. A strategy for the simplification of homonuclear two-dimensional NMR spectra. *J. Magn. Reson.* **78**, 588–593
62. Marion, D., Driscoll, P. C., Kay, L. E., Wingfield, P. T., Bax, A., Gronenborn, A. M., and Clore, G. M. (1989) Overcoming the overlap problem in the assignment of  $^1\text{H}$  NMR spectra of larger proteins by use of three-dimensional heteronuclear  $^1\text{H}$ - $^{15}\text{N}$  Hartmann-Hahn-multiple quantum coherence and nuclear Overhauser-multiple quantum coherence spectroscopy: Application to interleukin 1 beta. *Biochemistry* **28**, 6150–6156
63. Jeener, J., Meier, B. H., Bachman, P., and Ernst, R. R. (1979) Investigation of exchange processes by two-dimensional NMR spectroscopy. *J. Chem. Phys.* **71**, 45–46
64. Bax, A., and Davis, D. G. (1985) MLEV-17-based two-dimensional homonuclear magnetization transfer spectroscopy. *J. Magn. Reson.* **65**, 355–360
65. Kay, L. E., Torchia, D. A., and Bax, A. (1989) Backbone dynamics of proteins as studied by  $^{15}\text{N}$  inverse detected heteronuclear NMR spectroscopy: Application to staphylococcal nuclease. *Biochemistry* **28**, 8972–8979
66. Piotto, M., Saudek, V., and Sklenar, V. (1992) Gradient-tailored excitation for single-quantum NMR spectroscopy of aqueous solutions. *J. Biomol. NMR* **2**, 661–665
67. Grzesiek, S., and Bax, A. (1993) The importance of not saturating water in protein NMR. Application to sensitivity enhancement and NOE measurements. *J. Am. Chem. Soc.* **115**, 12593–12594
68. Delaglio, F., Grzesiek, S., Vuister, G. W., Zhu, G., Pfeifer, J., and Bax, A. (1995) NMRPipe: A multidimensional spectral processing system based on UNIX pipes. *J. Biomol. NMR* **6**, 277–293
69. Shen, Y., Delaglio, F., Cornilescu, G., and Bax, A. (2009) TALOS+: A hybrid method for predicting protein backbone torsion angles from NMR chemical shifts. *J. Biomol. NMR* **44**, 213–223
70. Koradi, R., Billeter, M., and Wuthrich, K. (1996) MOLMOL: A program for display and analysis of macromolecular structures. *J. Mol. Graph.* **14**, 29–32
71. Delano, W. L. (2002) Pymol: An open-source molecular graphics tool. *CCP4 Newsl. Pro. Crystallogr.* **40**, 82–92
72. Buck, M., Boyd, J., Redfield, C., MacKenzie, D. A., Jeenes, D. J., Archer, D. B., and Dobson, C. M. (1995) Structural determinants of protein dynamics: Analysis of  $^{15}\text{N}$  NMR relaxation measurements for main-chain and side-chain nuclei of hen egg white lysozyme. *Biochemistry* **34**, 4041–4055